Accelerated Coronary MRI with sRAKI: A Database-Free Self-Consistent Neural Network k-space Reconstruction for Arbitrary Undersampling

Seyed Amir Hossein Hosseini[1,2], Chi Zhang[1,2], Sebastian Weingärtner[1,2,3], Steen Moeller[2], Matthias Stuber[4,5], Kâmil Uğurbil[2], and Mehmet Akçakaya[1,2*]

[1]Electrical and Computer Engineering, University of Minnesota, Minneapolis, MN
[2]Center for Magnetic Resonance Research, University of Minnesota, Minneapolis, MN
[3]Department of Imaging Physics, Delft University of Technology, Delft, Netherlands
[4]Department of Radiology, University Hospital (CHUV) and University of Lausanne (UNIL), Lausanne, Switzerland
[5]Center for Biomedical Imaging (CIBM), Lausanne, Switzerland

*Corresponding Author

E-mail: akcakaya@umn.edu (MA)

Abstract

Purpose: To accelerate coronary MRI acquisitions with arbitrary undersampling patterns by using a novel reconstruction algorithm that applies coil self-consistency using subject-specific neural networks.

Methods: Self-consistent robust artificial-neural-networks for k-space interpolation (sRAKI) performs iterative parallel imaging reconstruction by enforcing self-consistency among coils. The approach bears similarity to SPIRiT, but extends the linear convolutions in SPIRiT to nonlinear interpolation using convolutional neural networks (CNNs). These CNNs are trained individually for each scan using the scan-specific autocalibrating signal (ACS) data. Reconstruction is performed by imposing the learned self-consistency and data-consistency, which enables sRAKI to support random undersampling patterns. Fully-sampled targeted right coronary artery MRI was acquired in six healthy subjects. The data were retrospectively undersampled, and reconstructed using SPIRiT, l_1-SPIRiT and sRAKI for acceleration rates of 2 to 5. Additionally, prospectively undersampled whole-heart coronary MRI was acquired to further evaluate reconstruction performance.

Results: sRAKI reduces noise amplification and blurring artifacts compared with SPIRiT and l_1-SPIRiT, especially at high acceleration rates in targeted coronary MRI. Quantitative analysis shows that sRAKI outperforms these techniques in terms of normalized mean-squared-error (~44% and ~21% over SPIRiT and ℓ_1-SPIRiT at rate 5) and vessel sharpness (~10% and ~20% over SPIRiT and l_1-SPIRiT at rate 5). Whole-heart data shows the sharpest coronary arteries when resolved using sRAKI, with 11% and 15% improvement in vessel sharpness over SPIRiT and l_1-SPIRiT, respectively.

Conclusion: sRAKI is a database-free neural network-based reconstruction technique that may further accelerate coronary MRI with arbitrary undersampling patterns, while improving noise resilience over linear parallel imaging and image sharpness over l_1 regularization techniques.

Keywords: coronary MRI, image reconstruction, accelerated imaging, parallel imaging, neural networks, deep learning

Introduction

Coronary artery disease (CAD) is the leading cause of death in the United States, accounting for one in seven deaths [1]. Coronary MRI provides a non-invasive and radiation-free diagnostic tool for CAD assessment [2], with a potential for repeated use. It is typically acquired with electrocardiogram (ECG) triggering during diastolic quiescence, where ~30-35 k-space lines are sampled per R-R interval [3–5]. When imaging the right coronary artery in a targeted manner [3], this leads to a ~3 minute nominal scan time. Since this scan time necessitates a free-breathing acquisition [6,7], respiratory motion compensation needs to be applied [4,5], typically with navigator gating [5,8], which further reduces the efficiency of the scans by ~2-3 fold, leading to a scan time of ~6-10 minutes. Alternatively, coronary MRI can be acquired with whole-heart coverage, which leads to a higher signal-to-noise ratio (SNR) [9,10], albeit at a longer nominal acquisition time of 6-8 minutes. The additional scan time overhead due to respiratory motion compensation often requires accelerated acquisitions, necessitating a trade-off with SNR [9,11].

Several strategies have been used to accelerate coronary MRI acquisitions such as parallel imaging [12,13], compressed sensing [14–16], and their combinations [17–23]. Recently, deep learning-based techniques [24–38] have also gained attention as a means to accelerate MRI acquisition. Numerous studies have designed neural network architectures that either establish an end-to-end nonlinear mapping from under-sampled k-space/distorted image to full k-space/undistorted image [25,27,28,31,33–35,37] or decompose an iterative optimization problem into (recurrent) deep learning blocks that learn a data-specific regularization [26,29,30,32,38]. A number of these studies also show support for parallel imaging with multi-coil data [24,26,29,31,36]. While these studies show promising results in accelerated MRI, there are

limitations regarding the training phase of reconstruction. Primarily, large datasets are required for training the neural networks, which is not readily available in all situations. This challenge has been partially addressed by transfer learning approaches, which pre-train neural networks on available large datasets and then fine-tune them on smaller datasets of specific applications [28,39]. However, transfer learning still requires training on fully-sampled data. The acquisition of fully-sampled training data in some applications e.g., in whole-heart coronary MRI, may be infeasible, since the scan time would become prohibitively long. Furthermore, training datasets may not include all pathologies of interest, which may lead to risks in generalizability for diagnosis [40]. These obstacles may hinder the clinical application of current transfer learning-based techniques to high-resolution cardiac MRI [40].

An alternative line of work considers subject-specific application of neural networks [24]. In this approach, called robust artificial-neural-networks for k-space interpolation (RAKI), several convolutional neural networks (CNN) are calibrated from scan-specific autocalibrating signal (ACS) data for improved interpolation of missing k-space lines. Thus, this method extends the linear convolutions used in GRAPPA [41], and was shown to increase noise resilience for uniform undersampling patterns, especially in low-SNR and high-acceleration rate regimes [24]. However, previous work has shown the benefits of random undersampling in high-resolution three-dimensional (3D) coronary MRI, for instance in the setting of compressed sensing [17]. For such undersampling patterns, iterative self-consistent parallel imaging reconstruction (SPIRiT) [42] provides a k-space interpolation approach for multi-coil data. SPIRiT utilizes multi-coil information by including a self-consistency term that ensures the interpolated k-space is consistent with itself according to the calibration kernels, along with a data-consistency term

in reconstruction. SPIRiT requires iterative processing in the reconstruction and is consequently more computationally-intensive than GRAPPA.

In this study, we exploit the notion of coil self-consistency in SPIRiT to enable RAKI with arbitrary undersampling. The proposed technique, called self-consistent RAKI (sRAKI), is evaluated in targeted and whole-heart coronary MRI, and compared with SPIRiT and ℓ_1-SPIRiT at various acceleration rates. This work has been partially presented in [43–46].

Methods

All imaging protocols were approved by the University of Minnesota institutional review board.

Written informed consent was obtained from all participants before each examination.

Calibration

For multi-coil k-space data with n_c coils, a k-space point in the j^{th} coil, $x_j(k_x, k_y, k_z)$ can be estimated as a function of distinct k-space points from all coils $i \in \{1, \dots, n_c\}$ within a neighborhood region of (k_x, k_y, k_z) [41,42]. In linear parallel imaging techniques, this function is modeled by a linear spatially shift-invariant convolution, and the convolutional kernels can be found by solving n_c linear least squares optimization problems [41,42]. In particular, SPIRiT uses these linear convolutional kernels to define a coil self-consistency rule that connects all the k-space elements with neighboring elements across all coils. However, it has been noted that a nonlinear mapping may be advantageous from a noise reduction perspective due to two factors. First, the shape and size of the neighborhood is heuristically set in practice [24], which may not capture all the required dependencies. Second, in contrast to typical least squares optimization problems, both the target and source points for the kernels in calibration are contaminated with

noise, and nonlinear functions have been shown to deal more effectively with such imperfections [24,47]. Thus, we propose to utilize CNNs that are calibrated (the terminology used for finding the self-consistency rule using ACS data) on ACS data of a single scan only to nonlinearly model the self-consistency in multi-coil k-space data.

In this study, a 4-layer CNN architecture was employed to learn the self-consistency rule among coils (Fig 1). In contrast to conventional RAKI, where separate CNNs were used for mapping to individual coils, a single CNN was used to map from all coils of multi-coil k-space onto itself, facilitating considerably reduced run time. For reduced computational complexity, 3D k-space data was first inverse Fourier transformed along fully-sampled k_x dimension. Subsequently 2D convolutional kernels were jointly calibrated on the resultant 2D slices of data [48]. The k-space data across all coils were normalized to have unit power as a preprocessing step to enable the use of a fixed learning rate. In addition, the complex k-space data was embedded to the real field, by concatenating the real and imaginary components of k-space along the coil dimension leading to $2n_c$ input and output channels. All layers, except the last one, were followed by rectifier linear units (ReLU) as activation functions. The kernel size at input and output layers was 5×5, while the hidden layers used 3×3 kernels. The number of output channels of different layers was 16, 8, 16 and $2n_c$, respectively. The network was designed such that the middle layer narrowed down to fewer output channels [49], since the CNN is prone to learn a trivial identity mapping from identical input and output training data, otherwise. A zero-padding strategy was used at each layer to maintain the size of input at the output after convolution. The network was trained by minimizing a MSE objective function using Adam optimizer [50]. A learning rate of 0.01 and maximum number of iterations of 1000 were used in training.

Fig 1. The CNN architecture to learn and enforce the coil self-consistency rule. The number of layer output channels is denoted by depth of blocks. All layers, except the last one, were followed by rectifier linear units (ReLU) as activation functions. The kernel sizes of the layers were 5×5, 3×3, 3×3 and 5×5, respectively. Each layer had 16, 8, 16 and $2n_c$ output channels, respectively. The 3D k-space data was first inverse Fourier transformed along fully-sampled k_x dimension. Subsequently 2D convolutional kernels were jointly trained on the ACS region of resultant 2D slices of data to learn the self-consistency rule.

Reconstruction

After calibrating the CNN on ACS data to learn the coil self-consistency rule, the following objective function is minimized to reconstruct k-space:

$$\arg\min_{\mathbf{x}} \|\mathbf{y} - \mathbf{D}\mathbf{x}\|_2^2 + \beta \|\mathbf{x} - \mathbf{G}(\mathbf{x})\|_2^2, \quad (1)$$

where $\mathbf{x}$ is the reconstructed k-space data across all coils, $\mathbf{y}$ is the noisy acquired data, $\mathbf{D}$ is the undersampling operator and $\mathbf{G}(\cdot)$ represents the calibrated CNN for self-consistency. The first term in the objective function in (1) ensures that the reconstructed k-space is consistent with acquired data. The second term enforces self-consistency in the reconstructed k-space according to the coil self-consistency rule that was learned by calibrating on the ACS data. The parameter β determines the balance between these two terms. Note that the main difference between sRAKI and RAKI is in this phase, where RAKI performs a one-time application of calibration kernels to

estimate the missing data, whereas sRAKI requires iterative optimization of Equation (1). Additional regularization terms can also be incorporated in (1), although this was not investigated in the current study to maintain the focus on multi-coil data processing.

The objective function in (1) was optimized using the Adam optimizer with a tuned learning rate of 2, for the same k-space normalization to unit power as before. We note that Adam only requires the gradient of the objective function with respect to the optimization variable **x,** which is the network input rather than network parameters in the reconstruction phase. Similar to network parameters, gradients with respect to the input were efficiently calculated through back-propagation by using the deep learning package Keras. In order to avoid a heuristic tuning of β, consistency with data was strictly enforced as in SPIRiT [42]. This led to gradients being calculated for non-acquired elements only while the rest of k-space was directly replaced with acquired data at each iteration. For comparison, SPIRiT using a conjugate gradient reconstruction was implemented with a 5×5 kernel [42]. l_1-SPIRiT was also implemented with additional a Daubechies-wavelet regularization [42], where the thresholding parameter was empirically tuned to 0.0005 of the maximum absolute wavelet coefficient. The number of reconstruction iterations were tuned separately for each technique and was set to 50 for SPIRiT and sRAKI, and 15 for l_1-SPIRiT. We note that l_1-SPIRiT converges at a faster rate, thus necessitating fewer iterations. All hyper-parameters were selected to optimize the performance of each technique both qualitatively and quantitatively.

Targeted Coronary MRI

All imaging was performed on a 3T Siemens Magnetom Prisma (Siemens Healthineers, Erlangen, Germany) system with a 30-channel receiver body coil-array. Targeted right coronary

artery (RCA) MRI was acquired on 6 healthy subjects (26.7 ± 2.9 years, 3 women). Scout images were followed by axial breath-hold cine bSSFP images to identify the quiescent period of the RCA, which was used for the trigger delay of coronary acquisitions. A low-resolution free-breathing ECG-triggered 3D coronary survey was acquired for slab orientation of the RCA imaging. Targeted RCA MRI was then acquired with a free-breathing ECG-triggered GRE sequence with imaging parameters: TR/TE=3.4/1.5ms, flip angle=20°, bandwidth=601 Hz/pixel, field-of-view (FOV)=300×300×48 mm^3, resolution=1×1×3 mm^3, navigator window=5 mm. The nominal scan time was 160 seconds at a heart rate of 60 bpm. T_2-preparation and a spectrally-selective fat saturation were utilized for improved contrast.

The 3D k-space data was exported and retrospectively undersampled with a Poisson disc pattern at acceleration rates 2, 3, 4, and 5 with a fully-sampled 40×10 ACS region in k_y - k_z plane. These under-sampled data were then reconstructed using SPIRiT, l_1-SPIRiT and sRAKI for comparison, with the implementations detailed above. Final images were obtained using root-sum-squares combination of all coil images. All algorithms were implemented in Python, and processed on a workstation with an Intel E5-2640V3 CPU (2.6GHz and 256GB memory), and an NVIDIA Tesla V100 GPU with 32GB memory. Additional comparisons for uniformly undersampled data are shown in Supporting Information S1 Fig, while different random undersampling patterns, and their reconstructions are depicted in Supporting Information S2 and S3 Figs, respectively.

Image Analysis

Quantitative analysis of the reconstructions was performed using normalized mean square error (NMSE) with respect to the fully-sampled reference, as well as normalized vessel sharpness

measurements. NMSE was calculated in image domain between a given reconstruction method and the fully-sampled reference, normalized by the energy of the reference. Vessel sharpness scores were calculated for both sides of the vessel using a Deriche algorithm [51]. Normalized vessel sharpness was calculated as the average score of both sides divided by the intensity at vessel center. A normalized vessel sharpness value closer to 1 represents a sharper vessel border. The NMSE and normalized vessel sharpness measurements of the different reconstructions were statistically compared across subjects using a nonparametric sign-rank test for each acceleration rate. A p-value of <0.05 was considered significant.

Whole-Heart Coronary MRI

Prospectively undersampled whole-heart coronary MRI was acquired on an additional subject (28 years, male) at an acceleration rate of 5 with a Poisson disc pattern. The same sequence parameters were used with FOV=300×300×106 mm^3, resolution=1.2×1.2×1.2 mm^3. The data were then reconstructed using SPIRiT, l_1-SPIRiT and sRAKI for comparison, with the same implementations described above. We note that this scenario poses a challenge for traditional machine learning algorithms that perform supervised learning on databases of fully-sampled data, as it is difficult to acquire high-quality fully-sampled whole-heart coronary MRI data. This is due to the long scan time of a fully-sampled acquisition, which leads to quality degradation due to drift and changes in the motion patterns. We also note that there have been some recent efforts to acquire fully-sampled whole-heart coronary MRI for this purpose, even though the acquisition time remains long [52].

Results

Fig 2 depicts reformatted images from a targeted coronary MRI dataset reconstructed using SPIRiT, l_1-SPIRiT and sRAKI techniques at retrospective acceleration rates 2, 3, 4, and 5. RCA is visualized at all rates for all methods. sRAKI has visibly less noise at high acceleration rates compared to SPIRiT and fewer blurring artifacts compared to l_1-SPIRiT. The reformatted images from a second subject, are shown in Fig 3 with similar results showing that sRAKI has visibly less noise at high acceleration rates. sRAKI demonstrates improved quality at higher acceleration rates, reducing noise amplification and blurring artifacts compared with other reconstruction methods.

Fig 2. Reformatted right coronary artery (RCA) images from a 3D targeted coronary MRI dataset. The data were retrospectively undersampled at rates 2, 3, 4, and 5 in the k_y - k_z plane and then reconstructed using SPIRiT, l_1-SPIRiT and sRAKI (top, middle and bottom rows). Fully-sampled images are also displayed in the first column as a reference for comparison. sRAKI is visually more robust to noise amplification and blurring artifacts at high acceleration rates compared to SPIRiT and l_1-SPIRiT, respectively. (RCA: right coronary artery; AO: Aortic Root)

Fig 3. Reformatted right coronary artery (RCA) images from another 3D targeted coronary MRI dataset. This data was also retrospectively undersampled at rates 2, 3, 4, and 5, and fully-sampled images are shown in the first column as reference. The difference between SPIRiT and sRAKI is visually evident at all acceleration rates for this subject with more apparent noise amplification. Furthermore, compared to l_1-SPIRiT, sRAKI is more robust to blurring artifacts with increasing acceleration rates. (RCA: right coronary artery; AO: Aortic Root)

Fig 4 Summarizes the mean and standard deviation of the NMSE and normalized vessel sharpness measurements for SPIRiT, l_1-SPIRiT and sRAKI across all subjects. sRAKI improves mean NMSE by 34%, 30%, 39%, 44% compared to SPIRiT, and 18%, 21%, 21% and 21% compared to l_1-SPIRiT for rates 2, 3, 4 and 5, respectively. Statistical analysis confirms that sRAKI significantly improves NMSE at all acceleration rates over both SPIRiT and l_1-SPIRiT. In terms of normalized vessel sharpness, sRAKI provides 7%, 9%, 11%, 10% improvement compared to SPIRiT and 4%, 5%, 13% and 20% improvement compared to l_1-SPIRiT for rates 2 to 5, respectively. The improvements over SPIRiT are statistically significant at rates 2 and 3, while improvements over l_1-SPIRiT are statistically significant at rates 3-5.

Fig 4. (a) Mean normalized mean squared error (NMSE) and (b) quantitative normalized vessel sharpness measures for all reconstructions of rates 2 to 5. Error bars represent standard deviation across subjects. sRAKI outperforms SPIRiT and l_1-SPIRiT at all rates for both metrics.

The improvements in NMSE are statistically significant at all rates over both SPIRiT and l_1-SPIRiT, whereas the improvements in vessel sharpness with sRAKI are significant at rates 2 and 3 over SPIRiT, and rates 3-5 over l_1-SPIRiT. Red lines mark significant differences in the graphs.

Fig 5 depicts the results of a prospectively 5-fold accelerated whole-heart coronary imaging. sRAKI yields an improved visualization of both the RCA and the left circumflex artery (LCX) compared to SPIRiT and l_1-SPIRiT. The normalized vessel sharpness measurements for this subject were 0.30, 0.31 and 0.33 for RCA and 0.25, 0.22, 0.28 for LCX with SPIRiT, l_1-SPIRiT and sRAKI reconstructions.

Fig 5. Reformatted coronal image from a prospectively 5-fold accelerated whole-heart coronary MRI dataset. The results show similar characteristics to targeted coronary MRI, where sRAKI reduces blurring with respect to l_1-SPIRiT, and noise amplification with respect to SPIRiT.

Discussion

In this study, we proposed a novel reconstruction method called sRAKI to accelerate coronary MRI. sRAKI trained subject-specific CNNs to learn a nonlinear coil self-consistency rule for

multi-coil k-space data. In the reconstruction phase, this learned self-consistency rule was enforced along with data-consistency constraints, similar to SPIRiT reconstruction. Thus, sRAKI enabled reconstruction with arbitrary undersampling patterns, an extension to RAKI [24], which was designed to handle uniform undersampling patterns only. A nonlinear calibration may capture further dependencies for learning coil self-consistency rule more effectively, when the shape and size of the neighborhood is heuristically set [24] and both the target and source points for the kernels in calibration are contaminated with noise [24,47]. In this study, this translated to considerable reduction of reconstruction noise compared to SPIRiT. In contrast to the recent machine learning-based MRI techniques [25–38], which require large training datasets, sRAKI is trained on scan/subject-specific ACS data.

We note that there have been other methods for performing k-space interpolation using machine learning [24,36,53]. In DeepSPIRiT [36], multi-coil k-space data from a training database is first pre-processed with coil compression to yield a similar number of channels. Subsequently, CNNs are trained for different regions of k-space, which are then applied in a multi-resolution approach. This method was shown to reduce aliasing, while difficulty with high-resolution content was also noted. Because this method uses a training database, it still requires fully-sampled training data, which is difficult to apply in whole-heart coronary imaging, and thus differs fundamentally from the sRAKI approach. An alternative method that more closely matches sRAKI was proposed in [53]. This method, proposed independently after the initial presentation of our work [43–46], extends the AC-LORAKS approach to CNNs, in a manner similar to RAKI [24] and sRAKI. LORAKI has shown promising results in brain imaging, and has not been studied in the context of coronary MRI.

Several modifications were made to RAKI [24]. First, RAKI employed separate CNNs to learn nonlinear mapping functions from zero-filled multi-coil k-space data to missing data of individual coils. Therefore, $2n_c$ CNNs were trained to learn a full mapping function from multi-coil data to itself. In the new setting, we exploited a single CNN with more hidden layers to learn the coil self-consistency rule jointly, considerably reducing run time. Second, RAKI was examined in only 2D scenarios, whereas sRAKI was implemented for 3D datasets with two phase encoding dimensions. Another major difference is concerned with the reconstruction phase in which RAKI interpolates missing data with no iterations, but sRAKI optimizes an objective function to enforce data-consistency and self-consistency among coils. This procedure, which is similar to the reconstruction phase of SPIRiT, increases the computational burden by requiring first-order derivative calculation in each iteration. However, the extra complexity is not limiting. In this study, calibration on targeted right coronary artery datasets took ~20 seconds for SPIRiT and l_1-SPIRiT, and ~40 seconds for sRAKI all on GPU implementations, although none of the implementations were fully optimized. In addition, the reconstruction phase on GPU took ~220, 120 and 100 seconds for SPIRiT, l_1-SPIRiT and sRAKI, respectively. sRAKI is also different from its previous version, in which a different reconstruction optimizer was used for 2D imaging [46]. In addition the 4-layer architecture of SPIRiT-RAKI in [43] is different from sRAKI, as the former applies 3D kernels on the whole 3D volume rather than training a single network with 2D kernels on 2D slices of the 3D volume. We observed that the latter further improves training by reducing the number of trainable parameters for the same amount of data.

In this study, the CNN parameters including the number of layers, the number of layer output channels and kernel sizes were empirically set to optimize the performance visually and quantitatively. Meanwhile, we noted that a simpler model would be more likely to generalize to

future data. Other parameters such as learning rates were also tuned to achieve the best performance across the coronary MRI data sets. We note that this set of parameters may not yield the best performance for imaging all organs. Therefore, similar to other techniques, a parameter tuning procedure may need to be performed prior to using sRAKI in other applications for an optimal performance.

Similar to SPIRiT, regularization terms can be included in the sRAKI objective function, in order to incorporate additional prior information, such as sparsity in transform domains [14–16]. However, these regularization parameters often need to be carefully tuned to avoid residual artifacts [16]. On the other hand, sRAKI without transform domain regularization, whose objective function requires no additional parameter tuning, showed desirable noise properties. The noise improvement in sRAKI is learnt from the coil geometry, and does not inherently include any assumptions about compressibility in transform domains. A combination of sRAKI with advanced regularizers bears potential for improved reconstruction quality in certain lower SNR scenarios (additional experiments for these scenarios are shown in Supporting Information S4 and S5 Figs), but this was beyond the scope of this work, which emphasized the multi-coil aspect of the data at the native acquisition SNR.

In addition to explicit regularization terms, some noise amplification reduction can be achieved by limiting the number of iterations for both SPIRiT and sRAKI, at the cost of incomplete unaliasing. The effect of early termination of reconstruction is most pronounced as residual blurring artifacts, which is particularly troublesome in the application of high-resolution coronary MRI. Thus, our main criterion for number of iterations was to assure that blurring artifacts were entirely removed before reconstruction noise started to be amplified. We further

observed that in contrast to ℓ_1-SPIRiT and sRAKI, the transition between residual blurring artifacts and amplified reconstruction noise was particularly fast for SPIRiT, which is due to lack of a regularization mechanism in SPIRiT, consistent with the literature on iterative SENSE [54]. In terms of quantitative evaluation, since NMSE is captured in the loss function, additional evaluation of image quality was incorporated using the vessel sharpness measurements, as is standard in coronary MRI [11,16,21].

Finally, while this work showed the feasibility of using sRAKI for accelerating coronary MRI, we have not comprehensively evaluated the failure modes and the residual artifacts, and how these would affect diagnostic decisions. Further study of these effects is warranted in patient populations to establish diagnostic utility, and will be explored in future research.

Conclusion

The proposed sRAKI reconstruction is a database-free CNN-based technique for self-consistent parallel imaging with arbitrary undersampling patterns, where the CNNs are trained on scan-specific ACS data. sRAKI is effective in accelerating coronary MRI, and improves reconstruction quality compared to regularized and non-regularized SPIRiT.

References

1. Benjamin EJ, Muntner P, Alonso A, Bittencourt MS, Callaway CW, Carson AP, et al. Heart Disease and Stroke Statistics-2019 Update: A Report From the American Heart Association. Circulation. 2019;139: e56–e528. doi:10.1161/CIR.0000000000000659

2. Kim WY, Danias PG, Stuber M, Flamm SD, Plein S, Nagel E, et al. Coronary magnetic resonance angiography for the detection of coronary stenoses. New England Journal of Medicine. 2001;345: 1863–1869.

3. Stuber M, Botnar RM, Danias PG, Sodickson DK, Kissinger KV, Cauteren MV, et al. Double-oblique free-breathing high resolution three-dimensional coronary magnetic resonance angiography. Journal of the American College of Cardiology. 1999;34: 524–531. doi:10.1016/S0735-1097(99)00223-5

4. Oshinski JN, Hofland L, Mukundan S, Dixon WT, Parks WJ, Pettigrew RI. Two-dimensional coronary MR angiography without breath holding. Radiology. 1996;201: 737–743. doi:10.1148/radiology.201.3.8939224

5. McConnell MV, Khasgiwala VC, Savord BJ, Chen MH, Chuang ML, Manning WJ, et al. Prospective adaptive navigator correction for breath-hold MR coronary angiography. Magnetic Resonance in Medicine. 1997;37: 148–152. doi:10.1002/mrm.1910370121

6. Edelman RR, Manning WJ, Burstein D, Paulin S. Coronary arteries: breath-hold MR angiography. Radiology. 1991;181: 641–643. doi:10.1148/radiology.181.3.1947074

7. Wielopolski PA, van Geuns RJ, de Feyter PJ, Oudkerk M. Breath-hold coronary MR angiography with volume-targeted imaging. Radiology. 1998;209: 209–219. doi:10.1148/radiology.209.1.9769834

8. Li D, Kaushikkar S, Haacke EM, Woodard PK, Dhawale PJ, Kroeker RM, et al. Coronary arteries: three-dimensional MR imaging with retrospective respiratory gating. Radiology. 1996;201: 857–863. doi:10.1148/radiology.201.3.8939242

9. Niendorf T, Hardy CJ, Giaquinto RO, Gross P, Cline HE, Zhu Y, et al. Toward single breath-hold whole-heart coverage coronary MRA using highly accelerated parallel imaging with a 32-channel MR system. Magnetic Resonance in Medicine. 2006;56: 167–176. doi:10.1002/mrm.20923

10. Weber OM, Martin AJ, Higgins CB. Whole-heart steady-state free precession coronary artery magnetic resonance angiography. Magnetic Resonance in Medicine. 2003;50: 1223–1228. doi:10.1002/mrm.10653

11. Etienne A, Botnar RM, Muiswinkel AMC van, Boesiger P, Manning WJ, Stuber M. “Soap-Bubble” visualization and quantitative analysis of 3D coronary magnetic resonance angiograms. Magnetic Resonance in Medicine. 2002;48: 658–666. doi:10.1002/mrm.10253

12. Hu P, Chan J, Ngo LH, Smink J, Goddu B, Kissinger KV, et al. Contrast-enhanced whole-heart coronary MRI with bolus infusion of gadobenate dimeglumine at 1.5 T. Magnetic Resonance in Medicine. 2011;65: 392–398. doi:10.1002/mrm.22706

13. Bi X, Carr JC, Li D. Whole-heart coronary magnetic resonance angiography at 3 Tesla in 5 minutes with slow infusion of Gd-BOPTA, a high-relaxivity clinical contrast agent. Magnetic Resonance in Medicine. 2007;58: 1–7. doi:10.1002/mrm.21224

14. Akçakaya M, Basha TA, Chan RH, Rayatzadeh H, Kissinger KV, Goddu B, et al. Accelerated contrast-enhanced whole-heart coronary MRI using low-dimensional-structure self-learning and thresholding. Magnetic Resonance in Medicine. 2012;67: 1434–1443. doi:10.1002/mrm.24242

15. Feng L, Coppo S, Piccini D, Yerly J, Lim RP, Masci PG, et al. 5D whole-heart sparse MRI. Magnetic Resonance in Medicine. 2018;79: 826–838. doi:10.1002/mrm.26745

16. Akçakaya M, Basha TA, Goddu B, Goepfert LA, Kissinger KV, Tarokh V, et al. Low-dimensional-structure self-learning and thresholding: Regularization beyond compressed sensing for MRI Reconstruction. Magnetic Resonance in Medicine. 2011;66: 756–767. doi:10.1002/mrm.22841

17. Akçakaya M, Basha TA, Chan RH, Manning WJ, Nezafat R. Accelerated isotropic sub-millimeter whole-heart coronary MRI: compressed sensing versus parallel imaging. Magnetic resonance in medicine. 2014;71: 815–822.

18. Piccini D, Feng L, Bonanno G, Coppo S, Yerly J, Lim RP, et al. Four-dimensional respiratory motion-resolved whole heart coronary MR angiography. Magnetic resonance in medicine. 2017;77: 1473–1484.

19. Forman C, Piccini D, Grimm R, Hutter J, Hornegger J, Zenge MO. High-resolution 3D whole-heart coronary MRA: a study on the combination of data acquisition in multiple breath-holds and 1D residual respiratory motion compensation. Magn Reson Mater Phy. 2014;27: 435–443. doi:10.1007/s10334-013-0428-x

20. Correia T, Ginami G, Cruz G, Neji R, Rashid I, Botnar RM, et al. Optimized respiratory-resolved motion-compensated 3D Cartesian coronary MR angiography. Magnetic Resonance in Medicine. 2018;80: 2618–2629. doi:10.1002/mrm.27208

21. Aitken AP, Henningsson M, Botnar RM, Schaeffter T, Prieto C. 100% Efficient three-dimensional coronary MR angiography with two-dimensional beat-to-beat translational and bin-to-bin affine motion correction. Magnetic Resonance in Medicine. 2015;74: 756–764. doi:10.1002/mrm.25460

22. Cruz G, Atkinson D, Henningsson M, Botnar RM, Prieto C. Highly efficient nonrigid motion-corrected 3D whole-heart coronary vessel wall imaging. Magn Reson Med. 2017;77: 1894–1908. doi:10.1002/mrm.26274

23. Munoz C, Cruz G, Neji R, Botnar RM, Prieto C. Motion corrected water/fat whole-heart coronary MR angiography with 100% respiratory efficiency. Magn Reson Med. 2019;82: 732–742. doi:10.1002/mrm.27732

24. Akçakaya M, Moeller S, Weingärtner S, Uğurbil K. Scan-specific robust artificial-neural-networks for k-space interpolation (RAKI) reconstruction: Database-free deep learning for fast imaging. Magnetic Resonance in Medicine. 2019;81: 439–453. doi:10.1002/mrm.27420

25. Wang S, Su Z, Ying L, Peng X, Zhu S, Liang F, et al. Accelerating magnetic resonance imaging via deep learning. 2016 IEEE 13th International Symposium on Biomedical Imaging (ISBI). IEEE; 2016. pp. 514–517.

26. Hammernik K, Klatzer T, Kobler E, Recht MP, Sodickson DK, Pock T, et al. Learning a variational network for reconstruction of accelerated MRI data. Magnetic resonance in medicine. 2018;79: 3055–3071.

27. Lee D, Yoo J, Tak S, Ye JC. Deep residual learning for accelerated MRI using magnitude and phase networks. IEEE Transactions on Biomedical Engineering. 2018;65: 1985–1995.

28. Han Y, Yoo J, Kim HH, Shin HJ, Sung K, Ye JC. Deep learning with domain adaptation for accelerated projection-reconstruction MR. Magnetic resonance in medicine. 2018;80: 1189–1205.

29. Aggarwal HK, Mani MP, Jacob M. MoDL: Model-Based Deep Learning Architecture for Inverse Problems. IEEE Transactions on Medical Imaging. 2019;38: 394–405. doi:10.1109/TMI.2018.2865356

30. Qin C, Schlemper J, Caballero J, Price AN, Hajnal JV, Rueckert D. Convolutional recurrent neural networks for dynamic MR image reconstruction. IEEE transactions on medical imaging. 2019;38: 280–290.

31. Kwon K, Kim D, Park H. A parallel MR imaging method using multilayer perceptron. Medical physics. 2017;44: 6209–6224.

32. Schlemper J, Caballero J, Hajnal JV, Price AN, Rueckert D. A Deep Cascade of Convolutional Neural Networks for Dynamic MR Image Reconstruction. IEEE Transactions on Medical Imaging. 2018;37: 491–503. doi:10.1109/TMI.2017.2760978

33. Yang G, Yu S, Dong H, Slabaugh G, Dragotti PL, Ye X, et al. DAGAN: Deep De-Aliasing Generative Adversarial Networks for Fast Compressed Sensing MRI Reconstruction. IEEE Transactions on Medical Imaging. 2018;37: 1310–1321. doi:10.1109/TMI.2017.2785879

34. Hyun CM, Kim HP, Lee SM, Lee S, Seo JK. Deep learning for undersampled MRI reconstruction. Phys Med Biol. 2018;63: 135007. doi:10.1088/1361-6560/aac71a

35. Eo T, Jun Y, Kim T, Jang J, Lee H-J, Hwang D. KIKI-net: cross-domain convolutional neural networks for reconstructing undersampled magnetic resonance images. Magnetic Resonance in Medicine. 2018;80: 2188–2201. doi:10.1002/mrm.27201

36. Cheng JY, Mardani M, Alley MT, Pauly JM, Vasanawala SS. DeepSPIRiT: Generalized Parallel Imaging using Deep Convolutional Neural Networks. Annual Meeting of the International Society of Magnetic Resonance in Medicine. 2018.

37. Han Y, Sunwoo L, Ye JC. k-Space Deep Learning for Accelerated MRI. IEEE Transactions on Medical Imaging. 2019; 1–1. doi:10.1109/TMI.2019.2927101

38. Aggarwal HK, Mani MP, Jacob M. MoDL-MUSSELS: Model-Based Deep Learning for Multishot Sensitivity-Encoded Diffusion MRI. IEEE Trans Med Imaging. 2019 [cited 17 Oct 2019]. doi:10.1109/TMI.2019.2946501

39. Hassan Dar SU, Çukur T. Transfer learning for reconstruction of accelerated MRI acquisitions via neural networks. Annual Meeting of the International Society of Magnetic Resonance in Medicine. 2018.

40. Eldar YC, III AOH, Deng L, Fessler J, Kovacevic J, Poor HV, et al. Challenges and Open Problems in Signal Processing: Panel Discussion Summary from ICASSP 2017 [Panel and Forum]. IEEE Signal Processing Magazine. 2017;34: 8–23. doi:10.1109/MSP.2017.2743842

41. Griswold MA, Jakob PM, Heidemann RM, Nittka M, Jellus V, Wang J, et al. Generalized autocalibrating partially parallel acquisitions (GRAPPA). Magnetic resonance in medicine. 2002;47: 1202–1210.

42. Lustig M, Pauly JM. SPIRiT: Iterative self-consistent parallel imaging reconstruction from arbitrary k-space. Magnetic Resonance in Medicine. 64: 457–471. doi:10.1002/mrm.22428

43. Hosseini SAH, Moeller S, Weingärtner S, Uğurbil K, Akçakaya M. Accelerated Coronary Mri Using 3D Spirit-Raki With Sparsity Regularization. 2019 IEEE 16th International Symposium on Biomedical Imaging (ISBI 2019). 2019. pp. 1692–1695. doi:10.1109/ISBI.2019.8759459

44. Hosseini S a. H, Moeller S, Weingärtner S, Uğurbil K, Akçakaya M. Accelerated Targeted Coronary MRI Using Sparsity-Regularized SPIRiT-RAKI. Annual Meeting of the International Society of Magnetic Resonance in Medicine. 2019 [cited 17 Jul 2019]. Available: https://par.nsf.gov/biblio/10095912-accelerated-targeted-coronary-mri-using-sparsity-regularized-spirit-raki

45. Hosseini S a. H, Moeller S, Weingärtner S, Uğurbil K, Akçakaya M. Accelerated Coronary MRI Using SPIRiT-RAKI with Gradient Descent-Based Self-Consistency. SCMR/ISMRM Co-Provided Workshop on the Emerging Role of Machine Learning in Cardiovascular Magnetic Resonance Imaging. 2019 [cited 17 Jul 2019]. Available: https://par.nsf.gov/biblio/10095906-accelerated-coronary-mri-using-spirit-raki-gradient-descent-based-self-consistency

46. Hosseini S a. H, Moeller S, Weingartner S, Uğurbil K, Akçakaya M. SPIRiT-RAKI: Scan-Specific Self-Consistency Neural Networks for Reconstruction Arbitrary k-space. ISMRM Workshop on Machine Learning Part II. 2018 [cited 17 Jul 2019]. Available: https://par.nsf.gov/biblio/10095903-spirit-raki-scan-specific-self-consistency-neural-networks-reconstruction-arbitrary-space

47. Chang Y, Liang D, Ying L. Nonlinear GRAPPA: A kernel approach to parallel MRI reconstruction. Magnetic Resonance in Medicine. 2012;68: 730–740.

48. Murphy M, Alley M, Demmel J, Keutzer K, Vasanawala S, Lustig M. Fast ℓ1-SPIRiT Compressed Sensing Parallel Imaging MRI: Scalable Parallel Implementation and Clinically Feasible Runtime. IEEE Trans Med Imaging. 2012;31: 1250–1262. doi:10.1109/TMI.2012.2188039

49. Liou C-Y, Cheng W-C, Liou J-W, Liou D-R. Autoencoder for words. Neurocomputing. 2014;139: 84–96. doi:10.1016/j.neucom.2013.09.055

50. Kingma DP, Ba J. Adam: A Method for Stochastic Optimization. San Diego, CA, USA: International Conference on Learning Representations; 2015.

51. Deriche R. Fast algorithms for low-level vision. IEEE transactions on pattern analysis and machine intelligence. 1990;12: 78–87.

52. Fuin N, Bustin A, Botnar RM, Prieto C. A Variational Neural Network for Whole-Heart Coronary MRA Reconstruction. Bellevue, WA USA: SCMR 22nd Annual Scientific Sessions; 2019.

53. Kim TH, Garg P, Haldar JP. LORAKI: Reconstruction of Undersampled k-space Data using Scan-Specific Autocalibrated Recurrent Neural Networks. Annual Meeting of the International Society of Magnetic Resonance in Medicine. 2019.

54. Pruessmann KP, Weiger M, Börnert P, Boesiger P. Advances in sensitivity encoding with arbitrary k-space trajectories. Magnetic Resonance in Medicine. 2001;46: 638–651. doi:10.1002/mrm.1241

Supporting Information

S1 Fig. Reformatted right coronary artery (RCA) images from a 3D targeted coronary MRI dataset. The data were uniformly undersampled retrospectively at rates 2×2, 3×2, 4×2 and 5×2 in $k_y - k_z$ plane, which are approximately equivalent to net acceleration rates 4, 5, 6 and 7 (including the ACS lines and an elliptical mask). These data were then reconstructed using GRAPPA, SPIRiT, ℓ_1-SPIRiT, RAKI and sRAKI (from top to bottom). Acceleration rate was set no higher than 2 for k_z dimension, since the size of data along this dimension was small (20 lines in total and 10 lines for ACS). For RAKI, a 3-layer network was designed with a kernel size of 2×2 (with dilations equaling acceleration rates to match the undersampled uniform pattern) for the first layer and a kernel size of 1×1 for subsequent layers. Note that this 2D undersampling is different from the original RAKI paper, thus the network architecture may be sub-optimal. The learning rate and number of epochs for RAKI were tuned to 0.05 and 2000 iterations, respectively. Fully-sampled images are also displayed in the first column as a reference for comparison. While RAKI is robust, GRAPPA is very sensitive to noise with increasing rates. In addition, RAKI outperforms SPIRiT, but RAKI and sRAKI perform comparatively, similar to the relationship between GRAPPA and SPIRiT

S2 Fig. Three k_y-k_z undersampling patterns were tested. Poisson disc (top), uniform-density random (middle) and variable-density random (bottom) with 4-fold acceleration.

S3 Fig. Reformatted right coronary artery (RCA) images from a 3D targeted coronary MRI dataset. The data were retrospectively undersampled with the three different patterns shown in Supporting Figure S2. These data were then reconstructed using SPIRiT, ℓ_1-SPIRiT and sRAKI. The results show that sRAKI is more resilient to noise amplification compared with SPIRiT, regardless of undersampling pattern.

S4 Fig. Noise sensitivity of the reconstruction methods are shown on reformatted right coronary artery images. Additive Gaussian noise was added to the datasets retrospectively, and the reported SNR was measured at aorta (signal power at aorta divided by noise power in an empty region of interest), with the original dataset having SNR of 50. The datasets were then retrospectively undersampled at rate 4 and reconstructed using SPIRiT, l_1-SPIRiT and sRAKI. sRAKI is more robust against noise of data compared with SPIRiT. However, noise amplification becomes evident with increasing levels of noise compared with l_1-SPIRiT.

S5 Fig. Normalized mean squared error (NMSE) of reconstruction across all subjects with 4-fold acceleration for the experiment setup described in Supporting Figure S4. Error bars represent standard deviation across subjects.

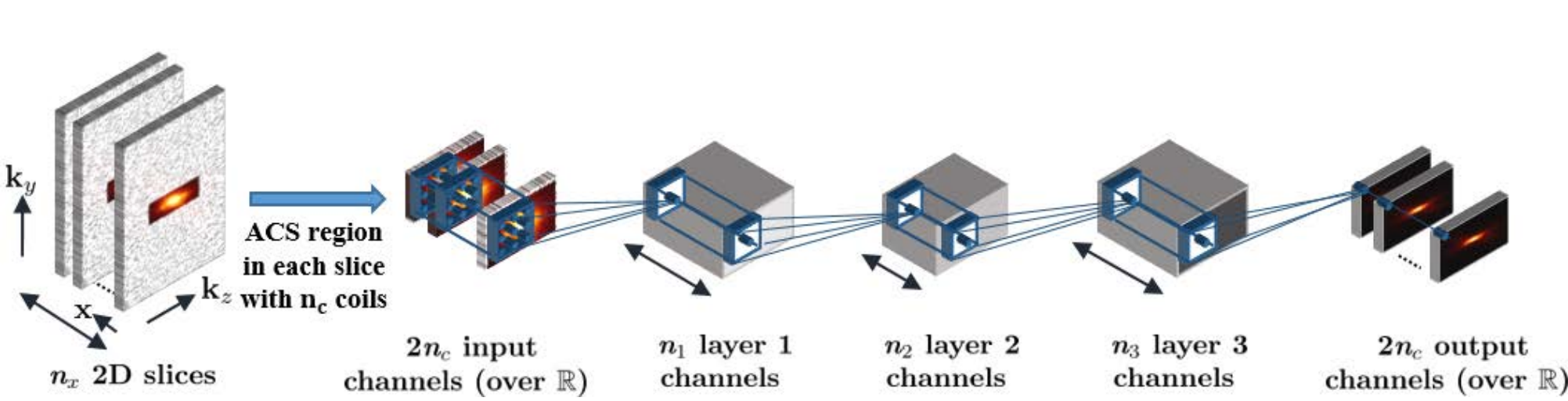
k_y
k_z
x
n_x 2D slices
ACS region
in each slice
with n_c coils
$2n_c$ input
channels (over $\mathbb{R}$)
n_1 layer 1
channels
n_2 layer 2
channels
n_3 layer 3
channels
$2n_c$ output
channels (over $\mathbb{R}$)

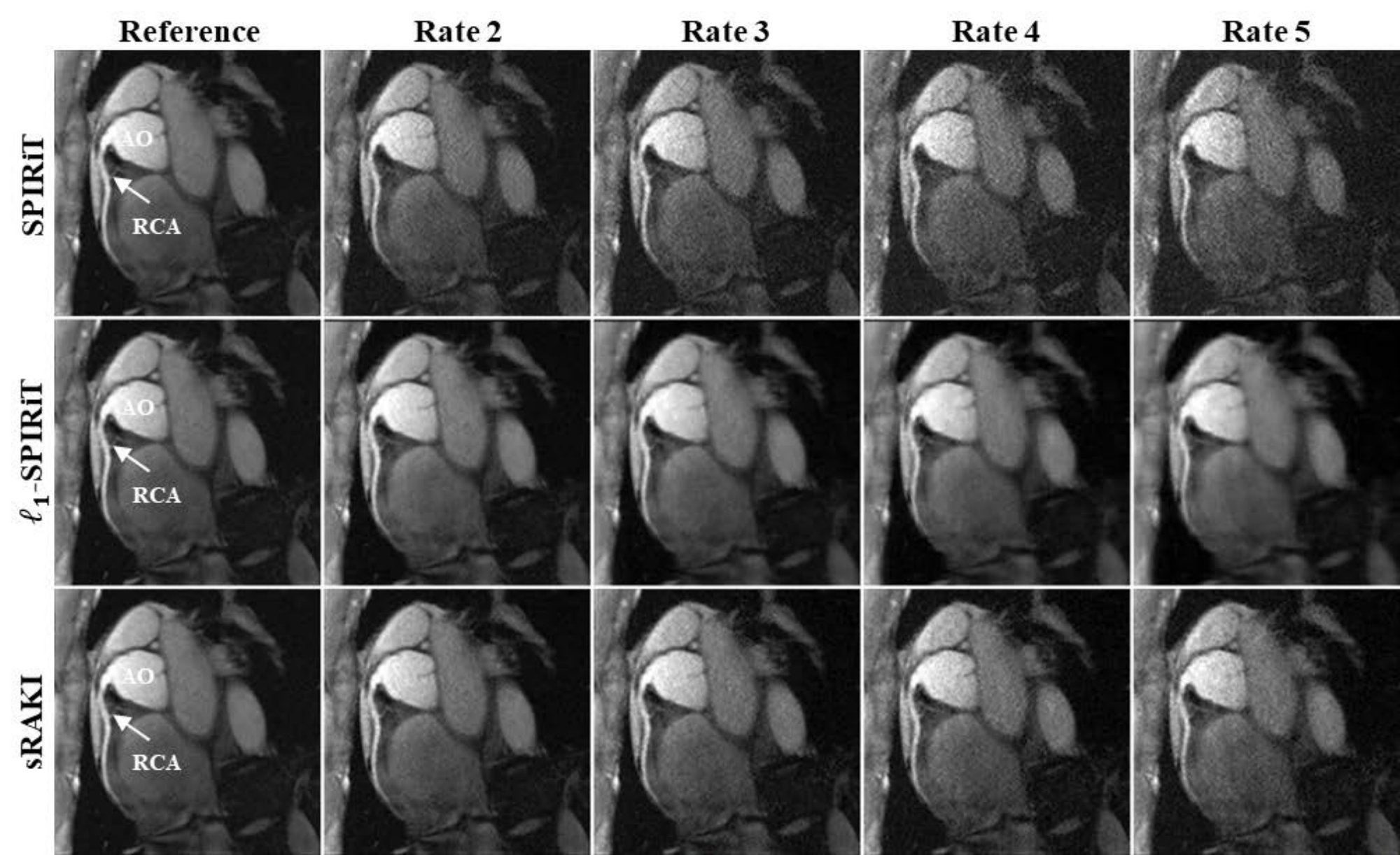
Reference
Rate 2
Rate 3
Rate 4
Rate 5
SPIRiT
ℓ_1-SPIRiT
sRAKI
AO
RCA
AO
RCA
AO
RCA

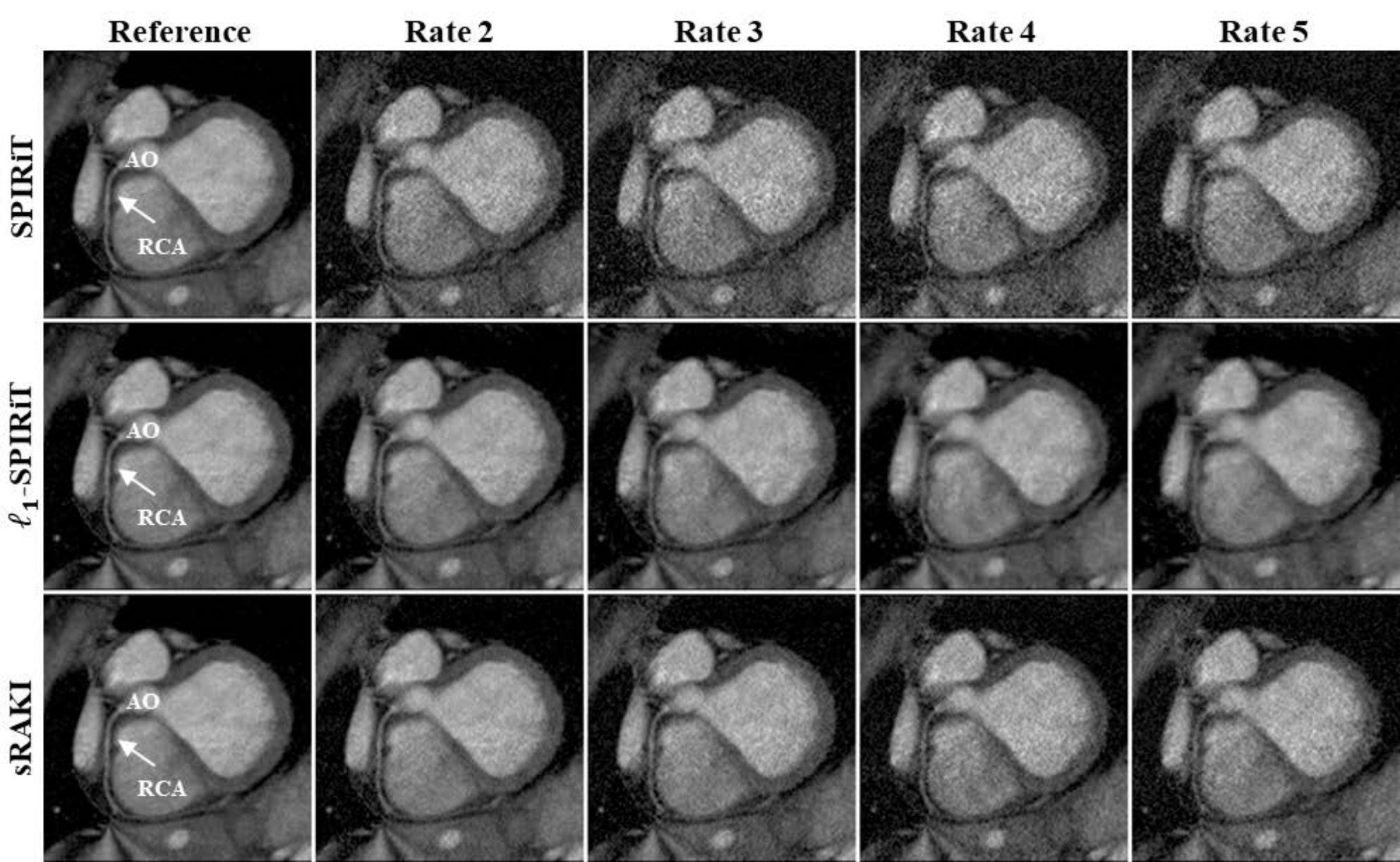
Reference
Rate 2
Rate 3
Rate 4
Rate 5
SPIRiT
ℓ_1-SPIRiT
sRAKI
AO
RCA
AO
RCA
AO
RCA

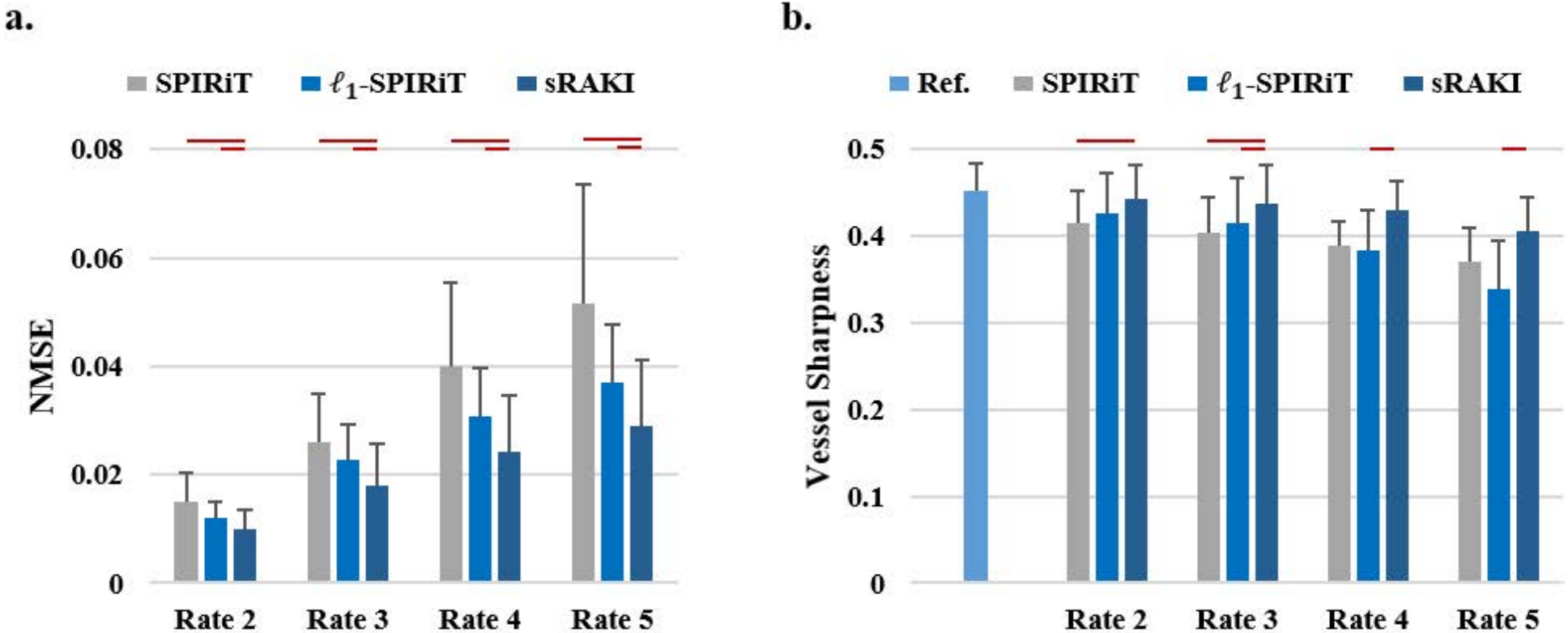
a.
SPIRiT
ℓ_1-SPIRiT
sRAKI
NMSE
0.08
0.06
0.04
0.02
0
Rate 2
Rate 3
Rate 4
Rate 5
b.
Ref.
SPIRiT
ℓ_1-SPIRiT
sRAKI
Vessel Sharpness
0.5
0.4
0.3
0.2
0.1
0
Rate 2
Rate 3
Rate 4
Rate 5

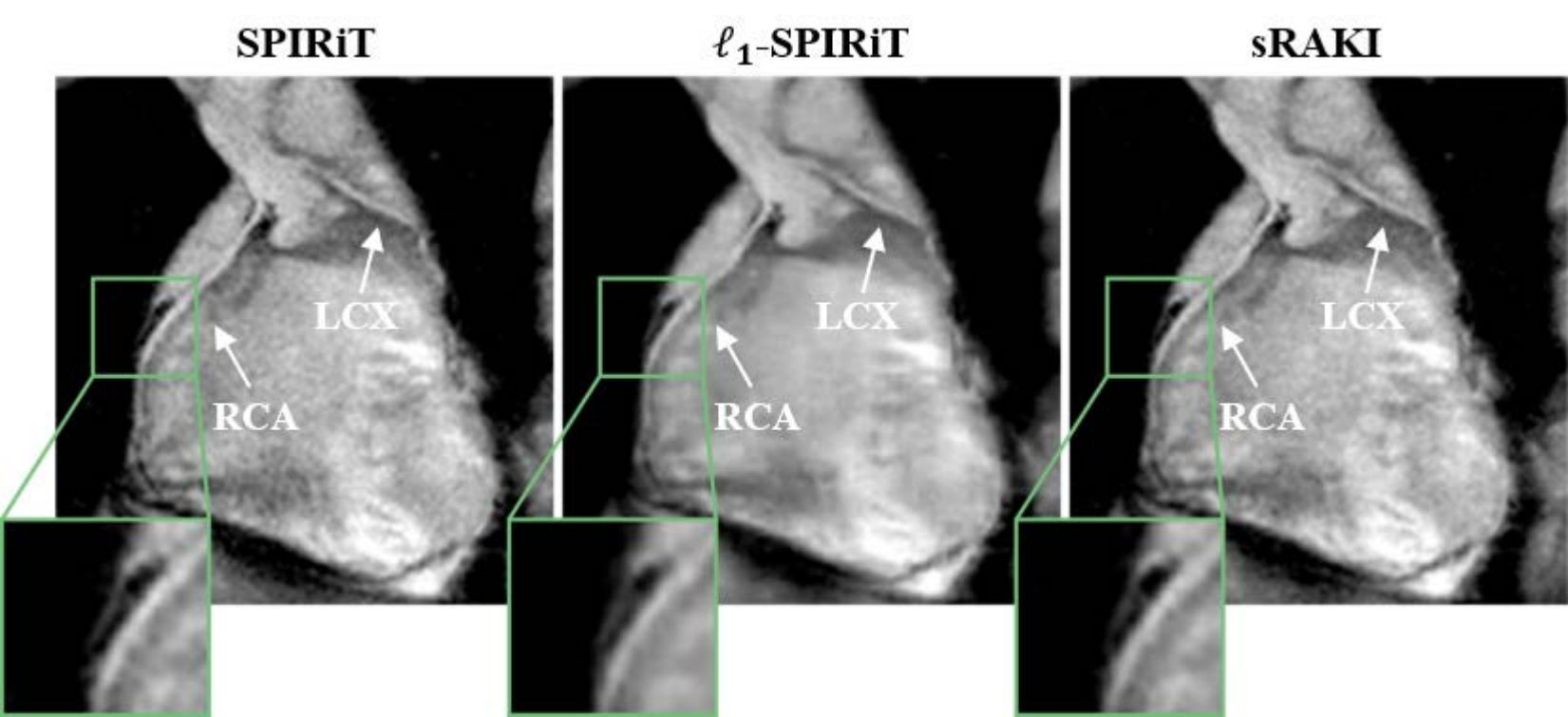
SPIRiT
ℓ_1-SPIRiT
sRAKI
LCX
RCA
LCX
RCA
LCX
RCA

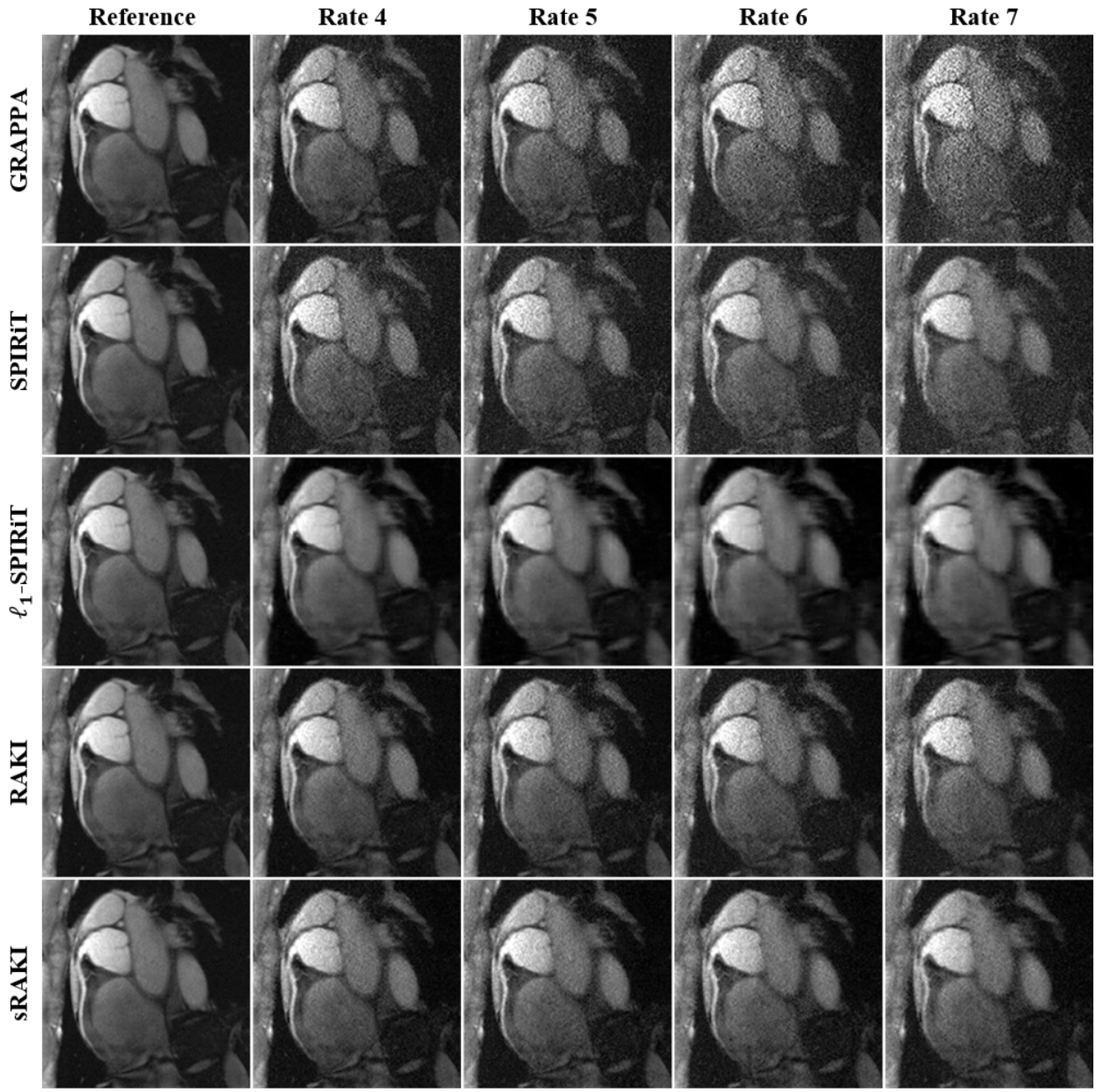

Supporting Figure S1: Reformatted right coronary artery (RCA) images from a 3D targeted coronary MRI dataset. The data were uniformly undersampled retrospectively at rates 2×2, 3×2, 4×2 and 5×2 in $k_y - k_z$ plane, which are approximately equivalent to net acceleration rates 4, 5, 6 and 7 (including the ACS lines and an elliptical mask). These data were then reconstructed using GRAPPA, SPIRiT, ℓ_1-SPIRiT, RAKI and sRAKI (from top to bottom). Acceleration rate was set no higher than 2 for k_z dimension, since the size of data along this dimension was small (20 lines in total and 10 lines for ACS). For RAKI, a 3-layer network was designed with a kernel size of 2×2 (with dilations equaling acceleration rates to match the undersampled uniform pattern) for the first layer and a kernel size of 1×1 for subsequent layers. Note that this 2D undersampling is different from the original RAKI paper, thus the network architecture may be sub-

optimal. The learning rate and number of epochs for RAKI were tuned to 0.05 and 2000 iterations, respectively. Fully-sampled images are also displayed in the first column as a reference for comparison. While RAKI is robust, GRAPPA is very sensitive to noise with increasing rates. In addition, RAKI outperforms SPIRiT, but RAKI and sRAKI perform comparatively, similar to the relationship between GRAPPA and SPIRiT.

Supporting Figure S2: Three 2D undersampling patterns were tested: Poisson disc (top), uniform-density random (middle) and variable-density random (bottom) with 4-fold acceleration.

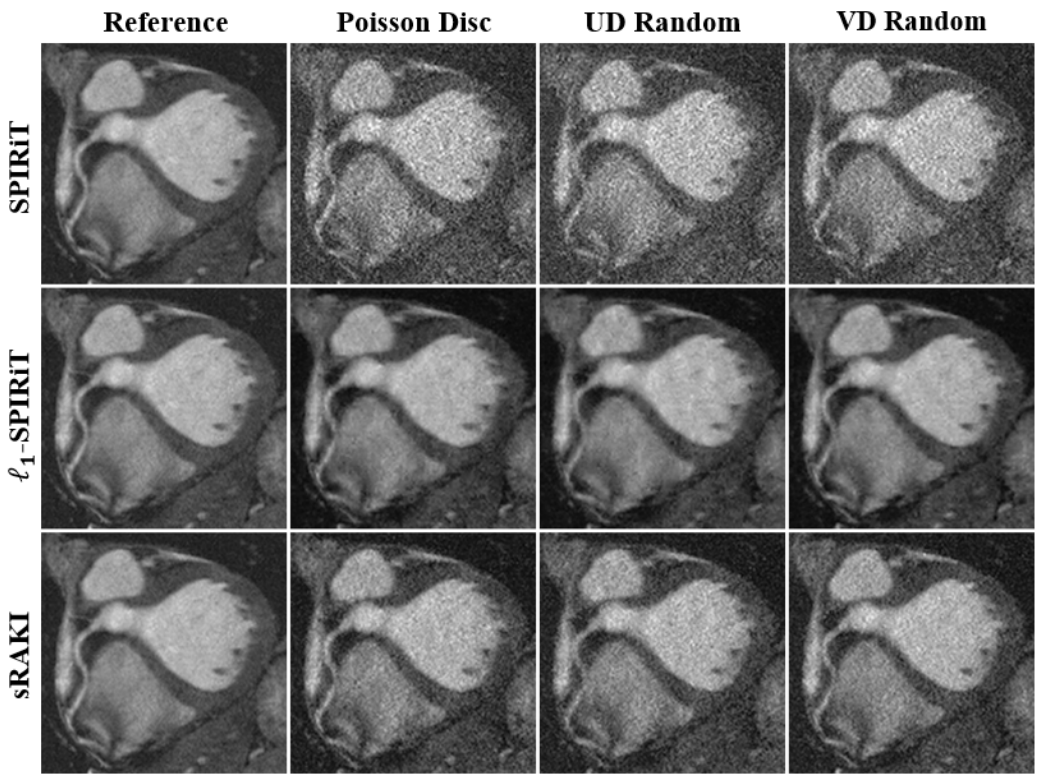

Supporting Figure S3: Reformatted right coronary artery (RCA) images from a 3D targeted coronary MRI dataset. The data were retrospectively undersampled with the three different patterns shown in Supporting Figure S2. These data were then reconstructed using SPIRiT, ℓ_1-SPIRiT and sRAKI. The results show that sRAKI is more resilient to noise amplification compared with SPIRiT, regardless of undersampling pattern.

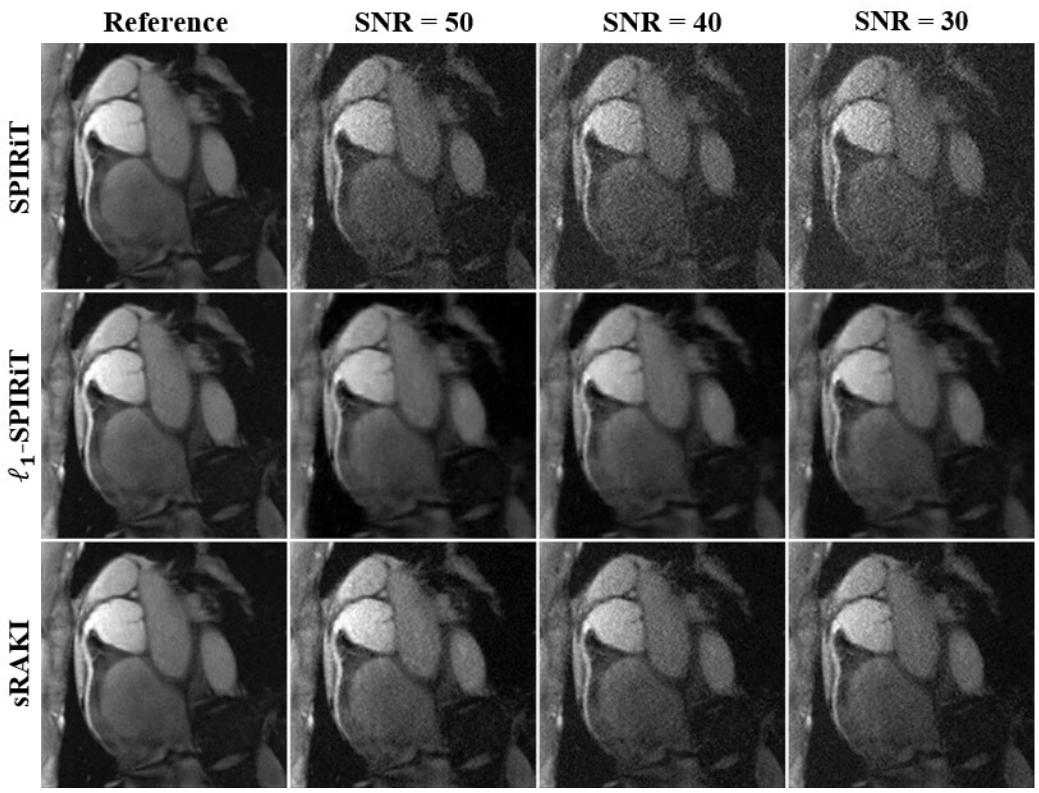

Supporting Figure S4: Noise sensitivity of the reconstruction methods are shown on reformatted right coronary artery images. Additive Gaussian noise was added to the datasets retrospectively, and the reported SNR was measured at aorta (signal power at aorta divided by noise power in an empty region of interest), with the original dataset having SNR of 50. The datasets were then retrospectively undersampled at rate 4 and reconstructed using SPIRiT, ℓ_1-SPIRiT and sRAKI. sRAKI is more robust against noise of data compared with SPIRiT. However, noise amplification becomes evident with increasing levels of noise compared with ℓ_1-SPIRiT.

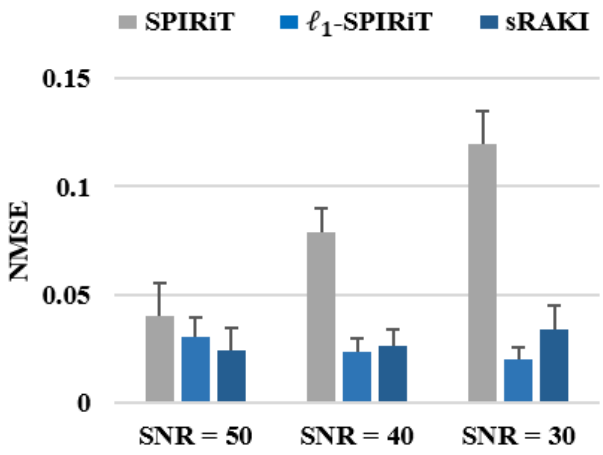

Supporting Figure S5: Normalized mean squared error (NMSE) of reconstruction across all subjects with 4-fold acceleration for the experiment setup described in Supporting Figure S4. Error bars represent standard deviation across subjects.